

# Development of Dynamic Estimators for Islanding Detection of Inverter-Based DG

Mohamed Al Hosani, *Member, IEEE*, Zhihua Qu, *Fellow, IEEE*, and H. H. Zeineldin, *Senior Member, IEEE*

**Abstract**—In this paper, a new islanding detection method (IDM) is proposed to dynamically estimate islanding occurrence. The proposed dynamic estimators estimate amplitudes and phase angles of the current injected by the grid at the point of common coupling with the distributed generation (DG) in addition to the DG's bus voltage. A distributed two-level algorithm is proposed to detect an islanding condition for single and multi-DG configurations. Analytical design and transient analysis are carried out for the islanding detection problem to determine the nondetection zone (NDZ) of the proposed islanding detection algorithm. A local low-frequency meshed communication network is sufficient to achieve distributed islanding detection capability for a general multi-DG network with negligible NDZ. It is shown through simulations that the proposed IDM can successfully distinguish an islanding condition from other disturbances that may occur in power system networks.

**Index Terms**—Distributed generation (DG), dynamic estimator, islanding detection methods (IDMs), nondetection zone (NDZ), quality factor and transient response.

## I. INTRODUCTION

ISLANDING refers to the case that a part of the grid, including a load and distributed generation (DG), is separated from the rest of the grid and continues to operate [1], [2]. Islanding detection methods (IDMs) are divided into three categories: 1) local passive [3]–[5]; 2) local active [4]–[6]; and 3) remote or communication-based techniques [4]. Among passive IDMs, undervoltage/overvoltage protection (UVP/OVP) and underfrequency/overfrequency protection (UFP/OF) are most commonly used due to simplicity and cost. Sandia frequency shift (SFS) and Sandia voltage shift (SVS) methods are examples of commonly used active IDMs. Some of the newly introduced active IDMs rely on injecting negative-sequence

current or disturbances in either the direct axis ( $d$ -axis) or the quadrature axis ( $q$ -axis) current controllers to detect islanding [7], [8]. However, active IDMs degrade the power quality (PQ) and negatively impact system stability [9]. Recently, hybrid IDMs that combine advantages of passive and active techniques are proposed in [10] and [11].

IDMs are evaluated using the concept of nondetection zone (NDZ), which can be represented using the power mismatch or phase criteria [12]–[17]. NDZs are the regions where the islanding detection scheme, under test, fails to detect islanding in a timely manner [12], [14]. As shown in [12]–[15], IDMs are analyzed in the steady state and, thus, are not taking into account transient analysis. According to the NDZ graphs in [12] and [13], the performance of active IDMs deteriorates as the load quality factor ( $Q_f$ ) increases; while passive IDMs typically have very large NDZ regions.

In this paper, the dynamics induced from an islanding condition are modeled and used to detect an islanding situation. A distributed two-level algorithm is proposed to detect the islanding condition for single and multi-DG networks. The proposed algorithm is implemented locally at each DG and at the point of common coupling (PCC) with the grid. For a general multi-DG structure, a local low-frequency meshed communication topology is sufficient to achieve robust islanding detection with negligible NDZ.

In [18], a dynamic estimator is presented to estimate only the grid current amplitude. In this paper, the design of the dynamic estimator in [18] is extended to also estimate the phase angle and, hence, resolve the singularity issue in [18]. Also, the proposed IDM in [18] is limited to single-DG system and does not consider the problem of multi-DG system with PCC that is far away from the DGs. Hence, a distributed multi-DG islanding detection algorithm is proposed in this paper to provide autonomous islanding detection capability at the DG level and the PCC level (microgrid level) such that various islanding conditions can be detected and identified (with the smallest NDZs possible). In addition, analysis is carried out in this paper to quantify the NDZ for the proposed IDM, and the proposed distributed algorithm is shown to be robust against different types of disturbances and power network events, such as three-phase short circuit, startup of induction motors, switching of capacitors, and load variations.

## II. ISLANDING TESTING CONDITIONS

A generic model for the transient anti-islanding study is shown in Fig. 1 and it resembles the anti-islanding testing diagram defined in UL 1741 and IEEE 929-2000 [1], [2]. The following assumptions are made in the subsequent analysis: 1)

Manuscript received March 08, 2014; revised July 08, 2014; accepted August 07, 2014. Date of publication October 13, 2014; date of current version January 21, 2015. This work was supported in part by the Masdar Institute of Science and Technology and in part by the U.S. National Science Foundation under Grant ECCS-1308928, in part by the U.S. Department of Transportation's under award DTRT13GUTC51, and in part by the U.S. Department of Energy under award DE-EE0006340. Paper no. TPWRD-00255-2014.

M. Al Hosani and H. H. Zeineldin, currently on leave from the Faculty of Engineering, Cairo University, Giza, Egypt, are with the Department of Electrical Engineering and Computer Science, Masdar Institute, United Arab Emirates (e-mail: mohalhosani@masdar.ac.ae; hzainaldin@masdar.ac.ae).

Z. Qu is with the Department of Electrical Engineering and Computer Science, University of Central Florida, Orlando, FL 32826 USA (e-mail: qu@ucf.edu).

Color versions of one or more of the figures in this paper are available online at <http://ieeexplore.ieee.org>.

Digital Object Identifier 10.1109/TPWRD.2014.2348654

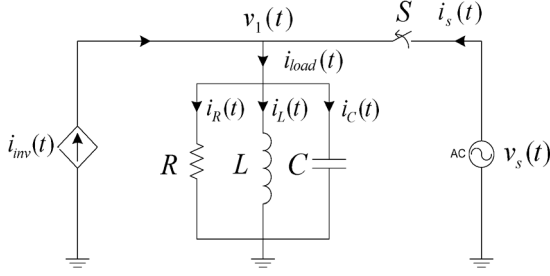


Fig. 1. Generic model for the transient islanding study.

The grid frequency and amplitude are  $v_s(t) = A_v \sin(\omega t + \varphi_v)$ , where  $\omega = 2\pi f$  is the grid frequency in radians/s and  $\varphi_v$  is equal to zero. 2) The steady state of the grid current is  $i_s(t) = A_s \sin(\omega t + \varphi_s)$ . 3) The dynamics of phase-locked loop (PLL) are fast and, hence, are considered negligible. 4) The inverter supplies active and reactive power by injecting current  $i_{inv}(t) = A_{inv} \sin(\omega_p t + \varphi_i)$ , where  $\omega_p$  is the frequency output of the PLL in radians/s. 5) The load is a parallel RLC load (and it meets islanding and nominal operation requirements). 6) The grid impedance is neglected.

### III. STEADY-STATE AND TRANSIENT ANALYSIS

For the RLC load, its quality factor ( $Q_f$ ) is defined as

$$Q_f = \omega_o RC = \frac{R}{\omega_o L} = R \sqrt{\frac{C}{L}} \quad (1)$$

where  $\omega_o = 2\pi f_o = 1/\sqrt{LC}$  is the resonance frequency of the RLC load in radians/s.

#### A. Mode 1: Switch (S) is Closed

The circuit dynamic equations before islanding occurs are

$$v_1(t) = v_s(t) = L \frac{di_L(t)}{dt}, \quad i_C(t) = C \frac{dv_1(t)}{dt}, \quad i_R(t) = \frac{v_1(t)}{R}. \quad (2)$$

It follows from assumption 1) that the inductor current is

$$i_L(t) = \int \frac{v_1(t)}{L} dt = -\frac{A_v}{\omega L} \cos(\omega t) + i_L(t_o) \quad (3)$$

where  $t_o$  is the initial time in seconds and  $i_L(t_o)$  is the initial inductor current. Similarly, the capacitor current is

$$i_C(t) = C \frac{dv_1(t)}{dt} = \omega C A_v \cos(\omega t). \quad (4)$$

A PLL is used to track the frequency of the PCC voltage  $v_1(t)$  and that frequency is utilized by the inverter to inject its current in phase with the voltage across the load to yield unity power factor operation. In other words, the PLL frequency before islanding is equal to the grid frequency ( $\omega_p = \omega$ ). It is worth mentioning that high-frequency components and distortion caused by the inverter's switching can be considered by improving the aforementioned model.

According to [12], the RLC circuit parameters for islanding condition are calculated as

$$R = \frac{V_r^2}{P_L}, \quad L = \frac{V_r^2}{2\pi f_o Q_f P_L}, \quad C = \frac{Q_f P_L}{2\pi f_o V_r^2},$$

$$A_{inv} = \frac{\sqrt{2}}{V_r} \sqrt{P_{inv}^2 + Q_{inv}^2}, \quad \varphi_i = -\text{atan2}(Q_{inv}, P_{inv}) \quad (5)$$

where  $\text{atan2}(\cdot)$  is a Matlab command that calculates the four-quadrant inverse tangent (arctangent),  $P_{inv}$  and  $Q_{inv}$  are the active and reactive powers supplied by the inverter before islanding, respectively;  $P_L$  is the active power absorbed by the RLC load before islanding, and  $V_r$  is the root mean square (rms) value of grid voltage.

Under zero initial conditions and upon neglecting PLL and controller dynamics, the steady-state grid current becomes

$$\bar{i}_s(t) = \bar{A}_s \sin(\omega t + \bar{\varphi}_s) \quad (6)$$

where

$$\bar{A}_s = \frac{\sqrt{2}}{V_r} \sqrt{\Delta P^2 + \Delta Q^2}, \quad \bar{\varphi}_s = -\text{atan2}(\Delta Q, \Delta P). \quad (7)$$

$\Delta P$  (which is equal to  $(P_L - P_{inv})$ ) is the active power mismatch between the load and inverter, and  $\Delta Q$  is the reactive power mismatch. Also,  $\Delta Q$  can be written in terms of the load's resonant frequency ( $f_o$ ) and quality factor ( $Q_f$ ) as follows:

$$\Delta Q = P_L Q_f \left( \frac{f_o}{f} - \frac{f}{f_o} \right) - Q_{inv}. \quad (8)$$

By applying Kirchhoff's Current Law (KCL) and Kirchhoff's Voltage Law (KVL) to the circuit shown in Fig. 1, the following differential equation is obtained:

$$\dot{v}_1(t) = a v_1(t) + b [i_s(t) + i_{inv}(t) - i_L(t)] \quad (9)$$

where  $a = (-1)/RC$  and  $b = 1/C$ . The solution to (9) is

$$v_1(t) = z_1(t) + z_2(t) \quad (10)$$

where

$$z_1(t) = e^{a(t-t_o)} z_1(t_o) + \int_{t_o}^t e^{a(t-\tau)} b i_s(\tau) d\tau, \\ z_2(t) = e^{a(t-t_o)} z_2(t_o) + \int_{t_o}^t e^{a(t-\tau)} b [i_{inv}(\tau) - i_L(\tau)] d\tau. \quad (11)$$

#### B. Mode 2: Switch (S) is Open

An islanding condition is simulated by opening the switch (S) in Fig. 1. The circuit equations after islanding are

$$v_1'(t) = L \frac{di_L'(t)}{dt} \neq v_s(t), \quad i_C'(t) = C \frac{dv_1'(t)}{dt}, \quad i_R'(t) = \frac{v_1'(t)}{R}. \quad (12)$$

Also, the inductor and capacitor steady-state currents after islanding are of the same form as (3) and (4). The PLL frequency after islanding is equal to the load resonant frequency if  $Q_{inv}$  is

equal to zero. In the case that  $Q_{\text{inv}}$  is not equal to zero, the PLL frequency after islanding is given by

$$f'_{\text{is}} = -\frac{f_o Q_{\text{inv}}}{2P_{\text{inv}} Q_f} + f_o \sqrt{\left(\frac{Q_{\text{inv}}}{2P_{\text{inv}} Q_f}\right)^2 + 1}. \quad (13)$$

In addition, similar to mode 1, the system dynamics can be described by the following differential equation:

$$\dot{v}'_1(t) = av'_1(t) + b[i'_{\text{inv}}(t) - i'_L(t)]. \quad (14)$$

And, the solution to (14) can be written as follows:

$$v'_1(t) \equiv z'_2(t) = e^{a(t-t_o)} v'_1(t_o) + \int_{t_o}^t e^{a(t-\tau)} b [i'_{\text{inv}}(\tau) - i'_L(\tau)] d\tau. \quad (15)$$

#### IV. DESIGN PROCEDURE

The grid current estimation is conducted at the PCC level and is expected to converge to zero when islanding occurs. In addition, the change in system dynamics from (9)–(14) will result in voltage variation if  $i_s$  is significant. Hence, by estimating the DG bus voltage amplitude, transient behavior could be detected locally due to islanding. Therefore, the main goal of this paper is to estimate grid current and DG bus voltage amplitudes in order to distinguish between islanding and other disturbances in power system networks.

In addition to the DG's local current measurement, the proposed design requires either load current measurement or PCC voltage measurement with the knowledge of the load or its estimate. In what follows,  $v_1$ ,  $\omega_p$ , and  $i_{\text{inv}}$  are available measurements to the estimator. From both Modes (1 and 2), the estimated version of the PCC voltage can be represented as

$$\hat{v}_1(t) = \hat{z}_1(t) + z_2(t) \quad (16)$$

where

$$\hat{z}_1(t) = e^{a(t-t_o)} \hat{z}_1(t_o) + \int_{t_o}^t e^{a(t-\tau)} b \hat{i}_s(\tau) d\tau \quad (17)$$

and  $\hat{i}_s(t) = \hat{A}_s \sin(\omega_p t + \hat{\varphi}_s)$  is the estimate of the current injected by the grid. As shown in (16), the estimate of  $v_1(t)$  includes two parts: one being reconstructed through known measurements ( $z_2$ ), and the other part being based on the estimate of the grid current ( $\hat{z}_1$ ). Since the solution of  $\hat{z}_1$  contains an integration term as shown in (17), a sliding integration window is used to implement the integration.

The proposed dynamic estimator utilizes the recursive least square algorithm. In particular, we rewrite (10) as

$$y_k(i) = \theta_k^T w_k(i) \quad (18)$$

where

$$\begin{aligned} w_1(i) &= \begin{bmatrix} \int_{t_{i-1}}^{t_{M+i-1}} e^{a(t_{M+i-1}-\tau)} b \sin(\omega_p \tau) d\tau \\ \int_{t_{i-1}}^{t_{M+i-1}} e^{a(t_{M+i-1}-\tau)} b \cos(\omega_p \tau) d\tau \end{bmatrix} \\ w_2(i) &= \begin{bmatrix} \sin(\omega_p t_{M+i-1}) \\ \cos(\omega_p t_{M+i-1}) \end{bmatrix}, \\ \theta_1 &= [A_s \cos(\varphi_s) \quad A_s \sin(\varphi_s)]^T, \\ \theta_2 &= [A_v \cos(\varphi_v) \quad A_v \sin(\varphi_v)]^T \\ y_1(i) &= v_1(t_{M+i-1}) - v_1(t_{i-1}) \\ &\quad - \int_{t_{i-1}}^{t_{M+i-1}} e^{a(t_{M+i-1}-\tau)} b [i_{\text{inv}}(\tau) - i_L(\tau)] d\tau, \\ y_2(i) &= v_1(t_{M+i-1}) \end{aligned} \quad (19)$$

and  $i = 1, 2, \dots, \infty$ ,  $k = 1, 2$ ,  $M = \text{floor}(W_L f_s)$  is the number of data points in a window of length  $W_L$  and floor is a Matlab command to round the number between brackets toward the nearest lower integer,  $t_{M+i-1} = t_o + (M+i-1) \times T_s$ ,  $t_{i-1} = t_o + (i-1) \times T_s$ ,  $f_s$  is the data sampling frequency, and  $T_s$  is the data sampling interval in seconds ( $T_s = 1/f_s$ ). In essence,  $\theta_k$  is the parameter vector to be estimated,  $w_k(i)$  is the regression vector, and  $y_k(i)$  is the measured signal. Equation (18) is obtained by expanding the estimated grid current and DG bus voltage forms into sine and cosine, by expressing both amplitudes and phases in linearly parameterized forms, and by utilizing the sliding window of integration. Equation (19) shows that generating the first estimates of  $w_1(i)$  and  $y_1(i)$  takes  $t_o + M \times T_s$  seconds.

Given the linearly parameterized expression in (18), standard algorithms can be applied to estimate the parameter vector  $\theta_k$ . The discrete recursive least square (RLS) algorithm with the forgetting factor is chosen to estimate the amplitudes and phase angles of the grid current and DG bus voltage. The RLS algorithm relies on the following equations [19]:

$$\begin{aligned} P_k(i+1) &= \frac{1}{\lambda_k} \left( P_k(i) - \frac{P_k(i) w_k(i) w_k^T(i) P_k(i)}{\lambda_k + w_k^T(i) P_k(i) w_k(i)} \right), \quad (20) \\ \hat{\theta}_k(i+1) &= \hat{\theta}_k(i) - P_k(i+1) w_k(i) [w_k^T(i) \hat{\theta}_k(i) - y_k(i)] \end{aligned} \quad (21)$$

where  $\hat{\theta}_k(i) = [\hat{\theta}_{k1} \hat{\theta}_{k2}]^T$  is the RLS estimated parameter vector for  $\theta_k \in R^2$  at the  $i$ th instant,  $e_k(i) = w_k^T(i) \hat{\theta}_k(i) - y_k(i)$  is the error,  $P_k(i)$  is the covariance matrix, and  $\lambda_k$  is the forgetting factor corresponding to the discount or length of memory.

Convergence of the algorithm is guaranteed since the regression vectors  $w_k(i)$  defined in (19) are persistently excited [19]. It follows from the RLS results that the estimates of grid current and DG bus voltage amplitudes (in per unit) and phases (in degrees) can be calculated as follows:

$$\begin{aligned} \hat{A}_s &= \frac{1}{I_{base}} \sqrt{\hat{\theta}_{11}^2 + \hat{\theta}_{12}^2}, \quad \hat{\varphi}_s = \frac{180}{\pi} \text{atan2}(\hat{\theta}_{12}, \hat{\theta}_{11}), \\ \hat{A}_v &= \frac{1}{V_{base}} \sqrt{\hat{\theta}_{21}^2 + \hat{\theta}_{22}^2}, \quad \hat{\varphi}_v = \frac{180}{\pi} \text{atan2}(\hat{\theta}_{22}, \hat{\theta}_{21}) \end{aligned} \quad (22)$$

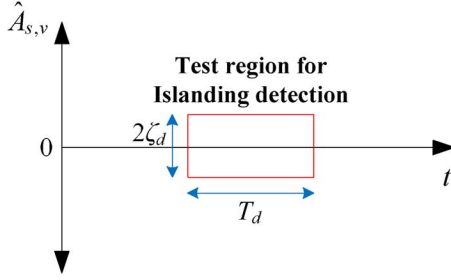


Fig. 2. Test region for achieving robust islanding detection.

where  $\{V_{\text{base}}, I_{\text{base}}\}$  is the pair of base voltage and current.

### V. ISLANDING DETECTION ALGORITHM

The algorithm of detecting an islanding condition employs a sliding rectangular test region of a time length  $T_d$  and with a width  $2\zeta_d$ , as shown in Fig. 2. The same testing region, but with a width of  $2\zeta_\varphi$ , is used in phase estimation. The following quantities can be defined as follows:

$$\begin{aligned} A_{\text{err}}^{s,v}(i) &= A_{\text{max}}^{s,v}(i) - A_{\text{min}}^{s,v}(i) \\ &= \max\left(\hat{A}_{s,v}(i:i+N_d)\right) - \min\left(\hat{A}_{s,v}(i:i+N_d)\right), \\ \varphi_{\text{err}}^s(i) &= \max(|\hat{\varphi}_s(i:i+N_d)|) - \min(|\hat{\varphi}_s(i:i+N_d)|) \end{aligned} \quad (23)$$

where  $i = 1, 2, \dots$  and  $N_d = \text{floor}(T_d f_s)$ .

Fig. 3 shows the flowchart of the proposed islanding detection algorithms. The parameters  $V_{\text{max}}$  and  $V_{\text{min}}$  are the upper and lower thresholds for UVP/OVP, respectively. The outcomes of both algorithms can be interpreted as follows:

$$L_{s,v}(i) = \begin{cases} 0 & \text{Islanding is detected} \\ 1 & \text{Normal operation} \\ 2 & \text{Oscillation or transition.} \end{cases} \quad (24)$$

It can be seen from Fig. 3(b) that a dynamic version of UVP/OVP is implemented locally at the DG side. The proposed DG-level algorithm provides local detection of both grid oscillation and islanding conditions. Hence, the DG-level algorithm plays a major role in reducing the communication requirement while achieving distributed islanding detection capability for a general multi-DG structure as will be shown in Section VII. However, the NDZ of the proposed DG-level algorithm is similar to UVP/OVP NDZ and is considered to be a very large NDZ [12]. Therefore, a PCC-level algorithm is proposed in Fig. 3(a) to significantly reduce the overall NDZ. A triggering variable  $H$  is used in the PCC-level algorithm to prevent premature islanding detection. Hence, the above logic distinguishes islanding from other transition cases, which prevents false islanding detection, improves islanding confirmation decision, and enhances robustness of the proposed IDM. For the simple case shown in Fig. 1, the PCC-level algorithm in Fig. 3(a) is also implemented locally at the DG side since the DG is assumed to have access to PCC information. As a result, both algorithms in Fig. 3 can detect islanding condition

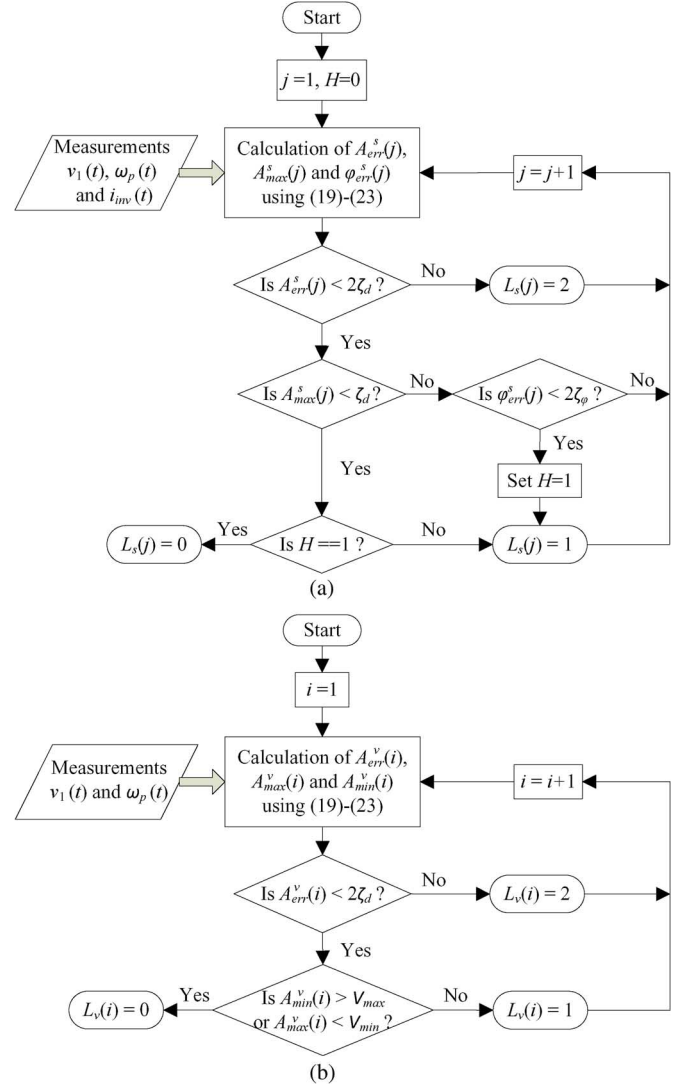


Fig. 3. Flowchart of the proposed islanding detection algorithms: (a) PCC-level algorithm. (b) DG-level algorithm.

while negligible NDZ can be achieved only by the PCC-level algorithm as will be shown in Section VI.

The DG is required to cease operation (unless microgrid operation is permitted) if either one of the algorithms presented in Fig. 3 detected islanding condition. It is recommended for an inverter to maintain its normal operation under grid oscillation in order to support loads and suppress grid oscillations. It is shown in Fig. 2 that threshold value  $\zeta_d$  (or  $\zeta_\varphi$ ) and window length  $T_d$  are standard parameters to achieve robust identification. In practice, the value of  $\zeta_d$  should be larger than the noise level such that steady-state normal operation ( $L_v = L_s = 1$ ) can be achieved for both algorithms during normal DG operations. Also, the window length should not be too small or too large because a very short window would be insufficient for islanding detection while a long window would confirm an islanding condition but introduce an unnecessary delay. Different  $\zeta_d$  values could be used for each algorithm in Fig. 3 if necessary and a single value is used for simplicity.

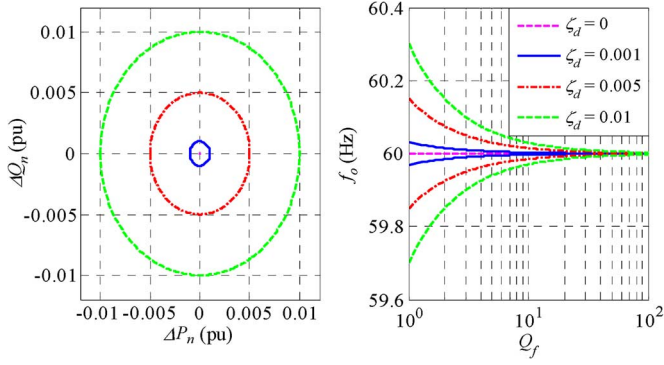


Fig. 4. NDZs of the proposed PCC-level algorithm for different values of  $\zeta_d$  in power mismatch space (left) and  $f_o - Q_f$  space (right).

## VI. NON-DETECTION ZONE OF PCC-LEVEL ISLANDING DETECTION ALGORITHM

The NDZ for the DG-level algorithm in Fig. 3(b) is similar to UVP/OVP NDZ which has been studied in [12] and [15]. However, the proposed algorithm will provide higher sensitivity to detect oscillation since it depends on instantaneous estimation of bus voltage amplitude rather than RMS values. It is worthy to note that available commercial relays have the capability of using either RMS or instantaneous values. On the other hand, a theoretical NDZ can be found for the PCC-level algorithm in Fig. 3(a) by studying the grid current steady-state behavior. The theoretical steady-state approximation of the grid current amplitude is given by (7). The NDZ boundary condition for the algorithm in Fig. 3(a) is given by

$$\bar{A}_{\text{spu}}^2 = \zeta_d^2 \quad (25)$$

where  $\bar{A}_{\text{spu}} = \bar{A}_s / I_{\text{base}}$ , and  $\zeta_d$  is the sensitivity parameter used in the PCC-level algorithm to detect the islanding condition.

One of the commonly used load spaces to represent the NDZ is the reactive-active power mismatch space [12]. The following equilibrium condition can be deduced from (25):

$$\Delta Q_n^2 + \Delta P_n^2 - \zeta_d^2 = 0 \quad (26)$$

where  $\Delta P_n = \Delta P / S_{\text{base}}$ , and  $\Delta Q_n = \Delta Q / S_{\text{base}}$ .

Active IDMs' performances depend upon the load's  $Q_f$  and hence the power mismatch space is inadequate to assess the performance of active IDMs [14]. Hence, the  $f_o - Q_f$  load space is proposed in [13]. Consider that a 1 kW inverter supplies only active power to the full load (i.e.,  $\Delta P = Q_{\text{inv}} = 0$ ). Then, the following equilibrium condition is obtained from (8) and (25):

$$f_o^4 - f^2 \left( 2 + \frac{\zeta_d^2}{Q_f^2} \right) f_o^2 + f^4 = 0. \quad (27)$$

The two positive roots of (27) determine the theoretical NDZ boundaries. Fig. 4 shows the NDZ for the proposed IDM for different values of  $\zeta_d$  in both the power mismatch and  $f_o - Q_f$  spaces. In Fig. 5, the NDZ for the proposed dynamic estimator IDM is compared with the UFP/OFP NDZ and the NDZ of the SFS (with  $cf_o = 0$  and  $k = 0.15$ ) [20].

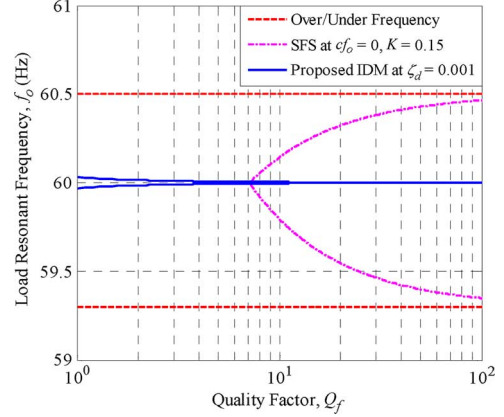


Fig. 5. Comparison of NDZs between different IDMs and the proposed PCC-level algorithm.

It is seen in Fig. 4 that, as  $\zeta_d$  becomes smaller, the theoretical NDZ for the PCC-level algorithm converges to a single point at (0,0) in the power mismatch space and that single point is equivalent to a single line at  $f_o = 60$  Hz in the  $f_o - Q_f$  space. The increase in NDZ width at low  $Q_f$  values is a result of small values of grid current amplitude as will be shown later by simulation. For design purposes, the value of  $\zeta_d$  is set equal to 0.001 pu in the simulations and a window of width 0.002 pu and length 35 ms (i.e., 2 cycles in 60 Hz) is shown to provide robust performance against disturbances and to successfully distinguish islanding from other disturbances (as will be shown in Section VIII). The NDZs, in Fig. 5, show that the proposed algorithm has a small NDZ width at low  $Q_f$  values and the overall size of NDZ for the proposed technique is much smaller than the UFP/OFP method. Therefore, the NDZ for the proposed IDM can be approximated by a single line at 60 Hz in  $f_o - Q_f$  space or a single point at (0,0) in  $\Delta Q_n - \Delta P_n$  space. It is worth mentioning that all the derivations for NDZ assume a proper choice of  $\zeta_\varphi$  in order to properly trigger  $H$  to indicate that both estimates of the grid current parameters converge to their steady state values under normal operation (before islanding).

## VII. DISTRIBUTED MULTI-DG ISLANDING DETECTION ALGORITHM

Let us assume the general multi-DG structure shown in Fig. 6.  $Z_{\text{line}}^j$  and  $Z_L^j$  are the line and local load impedances for the  $j$ th DG, respectively. Then, the following distributed algorithm is proposed. First, each DG estimates its own bus voltage ( $v_{DG}$ ) and produces  $L_u$  using the algorithm in Fig. 3(b), while the grid current estimation is carried out at PCC level and the algorithm in Fig. 3(a) is applied to determine the grid status. Then, there are several cases:

- 1) If the  $j$ th DG detected a local islanding condition ( $L_v^j = 0$ ), a signal is sent to PCC to check the status of the grid. While waiting for a response from PCC, the specific DG temporarily ceases its operation in order to protect its own equipment and maintain safety.
  - a) In case that PCC confirms islanding, a signal is sent through a meshed communication network so that all DGs can take appropriate action (e.g., de-energizing unless islanding operation is permitted).

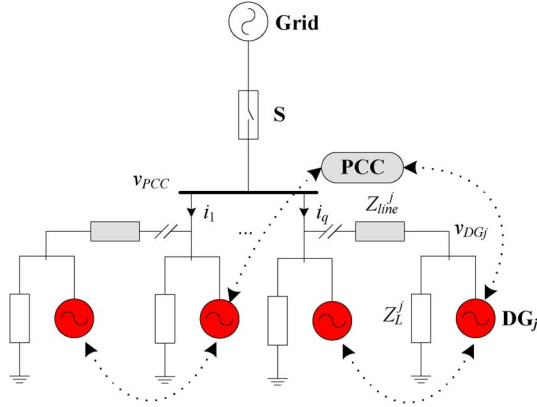


Fig. 6. General multi-DG structure for distributed multi-DG algorithm.

- b) If the PCC only detected grid oscillation, the DG shall receive this information from the PCC and in turn restore its operation, and the rest of DGs would maintain normal operation. If the  $j$ th DG couldn't restore normal operation and the local islanding condition is detected again, then the  $j$ th DG should cease its restoration and report its status to PCC.
- 2) If the  $j$ th DG detected oscillation ( $L_v^j = 2$ ), a signal is sent to PCC to check the status of the grid. The DG needs to check with PCC when either an islanding condition or oscillation behavior is locally detected. Meantime, the specific DG should maintain normal operation.
  - a) In case that PCC confirms islanding, a signal is sent to all DGs within the microgrid to take an action.
  - b) If the PCC only detected grid oscillation, then the  $j$ th DG would maintain normal operation.
- 3) If the PCC first detects islanding, it shall send the information to all DGs within the microgrid.

At PCC level, the information required are the currents of all branches that are directly connected to PCC ( $i_1, \dots, i_q$ ) in addition to the PCC voltage frequency. Individually, each DG will require its own bus voltage information. The PCC voltage frequency tracked by PLL is utilized in the grid current estimator while the frequency of local DG bus voltage is used for local voltage estimator. The overall NDZ of the proposed algorithm is similar to the PCC algorithm NDZ provided that the network has a proper communication topology with PCC.

This distributed islanding detection scheme (with negligible NDZ) can be implemented if the microgrid has a secure low-bandwidth meshed communication network (illustrated by Fig. 6). There are two main factors that will affect the islanding detection time and they are: the total propagation time, and the algorithm(s) processing time. The total propagation time includes the frame capture and sequencing, link delay, queuing delay, and node processing delay for transferring a signal from the  $j$ th DG to PCC and then back to the  $j$ th DG. Hence, the speed requirement for the communication network is at most 2 second for the total detection time as specified by IEEE 929-2000 in [1]. The other requirement of the communication system in terms of design is that DG should be able to identify

the source of the originated signal (whether it is PCC or other DGs). Communication requirement for such distributed algorithms can be found in [21]. It is important to note that when DGs are allocated close to each other, communication is no longer needed and the proposed scheme becomes completely passive. For large networks in which DGs are far away from each other and from the PCC as shown in Fig. 6, the required communication scheme is local (within the microgrid) and has minimum requirements in terms of frequency and bandwidth (since the only information exchanged is the detection of oscillation or islanding conditions).

## VIII. SIMULATION RESULTS

The system under study for the first two subsections consists of a 1 kW inverter-based DG connected to an  $RLC$  load and a grid as illustrated in Fig. 1. The system is simulated in MATLAB/Simulink. The performance of the developed estimators during islanding transients is studied under three loading conditions. The three loading conditions are:

- 1)  $RLC$  load that approximately resonates at 60 Hz with  $Q_f = 2.5$  and absorbs approximately 1 kW;
- 2)  $RLC$  load that approximately resonates at 59.6 Hz with  $Q_f = 2.5$  and absorbs approximately 1 kW;
- 3)  $RLC$  load that approximately resonates at 60 Hz with  $Q_f = 2.5$  and absorbs approximately 0.95 kW.

The loads chosen represent cases where other IDMs might fail to detect an islanding condition. For simulation purposes, microgrid operation is permitted and the forgetting factor ( $\lambda_k$ ) is set to 0.9 for all simulation cases. This value was chosen in order to make the estimator more sensitive to fast dynamics and to reduce the amount of memory required by both algorithms. The upper and lower thresholds of UVP/OVP are set to 1.1 and 0.88 per-unit, respectively. The rest of parameters used for simulation are:  $S_{\text{base}} = 1$  kVA,  $V_{\text{base}} = 170$  V,  $I_{\text{base}} = 11.8$  A,  $V_r = 120$  V,  $f = 60$  Hz,  $f_s = 7.68$  kHz,  $W_L = 8.3$  ms,  $T_d = 35$  ms,  $P_k(0) = 100$ ,  $\zeta_d = 0.001$  p.u., and  $\zeta_\varphi = 1^\circ$ .

### A. Detectability and Convergence Under Load Cases

At  $t = 2$  s, the grid switch was opened to examine the response of the dynamic estimator during islanding. Fig. 7 shows the responses of estimated DG bus voltage amplitude ( $\hat{A}_v$ ), estimated grid current amplitude ( $\hat{A}_s$ ), DG algorithm output ( $L_v$ ), and the PCC algorithm output ( $L_s$ ) for all the load cases. As seen in Fig. 7, case 1 is theoretically undetectable by both algorithms but practically inconsequential due to the perfect match in power, voltage and frequency between load and inverter. Therefore, the grid will not supply any active or reactive power and the amplitude of current injected by the grid is almost zero. Hence, no significant variation is detected in the DG bus voltage ( $L_v = 1$ ) during islanding. Cases 2 and 3 are detectable by the PCC algorithm although they lie within the NDZs of UFP/OFP and UVP/OVP, respectively. The NDZ of UFP/OFP is shown in Fig. 5, and it can be seen that case 2 lies within its NDZ. The NDZ for UVP/OVP is given in Fig. 3 in [12] and it can be seen that the point of  $\Delta P = -5\%$  and  $\Delta Q = 0$  (i.e., case 3) is obviously located inside the NDZ of UVP/OVP. When the grid is disconnected,  $\hat{A}_s$  converged to

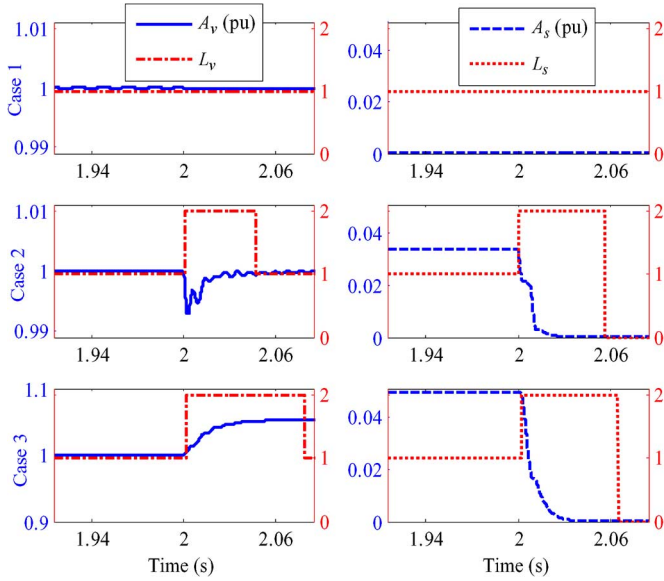


Fig. 7. Responses of both estimated amplitudes and algorithms' outputs for all of the load cases.

zero within approximately 20 and 30 ms for cases 2 and 3, respectively. The required time to confirm islanding conditions by PCC algorithm for cases 2 and 3 are 56.6 and 65.2 ms, respectively. Also, there is an initial delay of 43.2 ms or 2.6 cycle ( $W_L$  plus  $T_d$ ) to produce the first value of  $L_s$ . On the other hand, the DG-level algorithm detected oscillation ( $L_v = 2$ ) for cases 2 and 3. The oscillation detected for case 2 is a result of dynamic changes of voltage frequency from 60 to 59.6 Hz. For case 3,  $\hat{A}_v$  converged to a value of 1.05 p.u. after islanding and, hence, a transient behavior has been detected for this case as well. Furthermore, the proposed estimators provide good amplitude estimation with maximum steady-state errors at the level of  $0.5e-3$  for all of the cases studied. In addition to islanding detection, the flow direction of grid active and reactive power can be determined through the following steady-state relation:

$$\text{sign}(\Delta Q) = \text{sign}(-\hat{\theta}_{12}), \quad \text{sign}(\Delta P) = \text{sign}(\hat{\theta}_{11}). \quad (28)$$

The relation in (28) might produce incorrect results at steady state when  $\Delta P$  or  $\Delta Q$  is equal to zero. Therefore, a small threshold area around zero can be used to eliminate this problem. The grid in case 2 absorbs reactive power only, whereas it absorbs active power only for case 3.

### B. Effect of $Q_f$

The *RLC* load condition of case 2 will be used to study the effect of  $Q_f$  on both estimators and algorithm outputs responses. Fig. 8 shows the effect of different  $Q_f$  values on  $\hat{A}_v$ ,  $\hat{A}_s$ ,  $L_v$ , and  $L_s$ . From Fig. 8, it is noticed that high  $Q_f$  values resulted in higher  $\hat{A}_s$  values since loads with high  $Q_f$  value will require more support from the grid than loads with low  $Q_f$  value. This explains the reduction in NDZ size with the increase in  $Q_f$  values as shown in Fig. 4. However, larger  $\hat{A}_s$  value will require a slightly larger time to converge to zero since the decaying speed, when grid is disconnected, is mainly determined

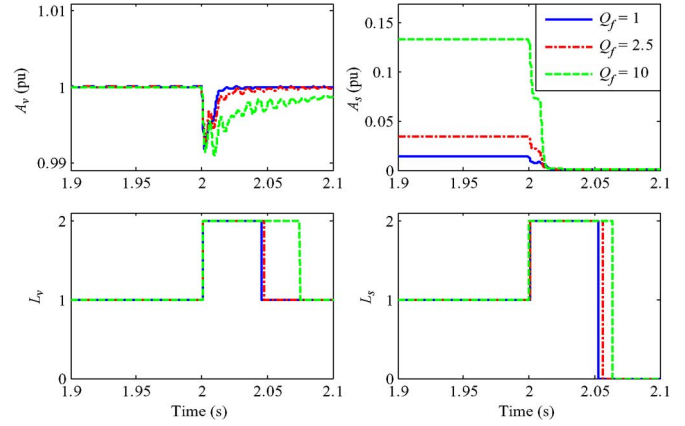


Fig. 8. Effect of different  $Q_f$  values on estimated amplitudes and algorithms' outputs responses.

by the forgetting factor of the RLS algorithm. Hence, the required time for the PCC-level algorithm to confirm islanding is 52.6, 56.6, and 63.7 ms for  $Q_f$  values equal to 1, 2.5, and 10, respectively. Typically, islanding detection methods are tested for loads with  $Q_f$  close to 1.

### C. IEEE 34-Bus Network

The standard IEEE 34-bus distribution network will be used to test the effectiveness of the proposed multi-DG algorithm. DigSilent, which is a very powerful program for studying and integrating power system networks, will be used for simulation. The detail of the parameters used in this network can be found in [21] and [22]. In [21], sixteen Photovoltaic DGs are integrated at different buses in the IEEE 34-bus and Fig. 9 shows a portion of the resulting network under study. The three-phase base power is 1 MVA and the line-to-line rms base voltage is 24.9 kV. Measurements are taken at buses (B) and (C) where the following cases are simulated:

- 1) A microgrid formation or islanding condition taking place at bus (C) by disconnecting line d at  $t = 2$  s.
- 2) A three-phase short circuit taking place at point (A) at  $t = 2$  s and clears out within 0.03 s.
- 3) A 0.5 MW induction motor switching on at  $t = 2$  s and off at  $t = 8$  s at bus (D).
- 4) A 1.0 MVAR capacitor switching on at  $t = 2$  s and off at  $t = 5$  s at bus (C). Also, a 1 MW +  $j1$  MVAR load switches on at  $t = 8$  s and off at  $t = 11$  s at bus (B).

The added induction motor, capacitor, and load in cases 3 and 4 are not shown in Fig. 9. Since the capacitor switching in case 4 is applied to PCC bus (C), the switching capacitance information should be adapted in the PCC-level algorithm to provide correct estimation for the grid current. Fig. 10, 11, and 12 show the responses of estimated DG bus voltages ( $\hat{A}_v^{B,C}$ ) with its local algorithms' outputs ( $L_v^{B,C}$ ) for buses (B) and (C) in addition to  $\hat{A}_s$  and  $L_s$  for all simulated cases. The DGs' local voltages at buses (B) and (C) are almost similar and hence are plotted using a single legend. Results show that the PCC-level algorithm distinguishes islanding condition ( $L_s = 0$ ) from three-phase short circuit, startup of induction motor,

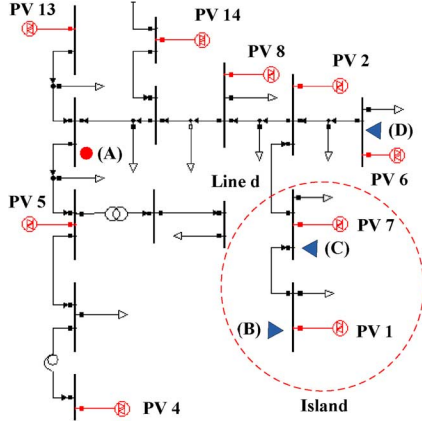


Fig. 9. Partial diagram of the IEEE 34-bus network.

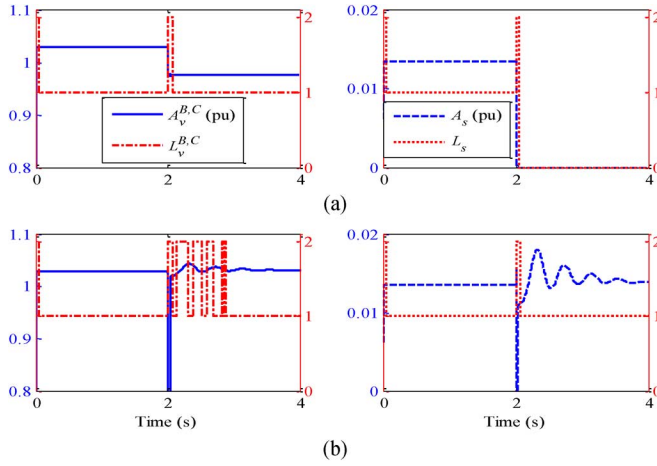
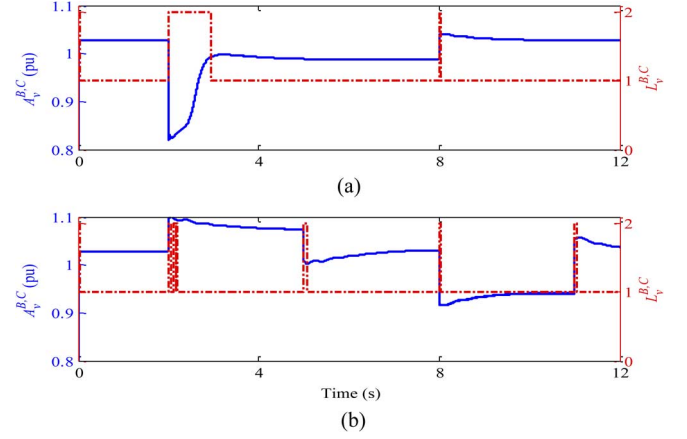
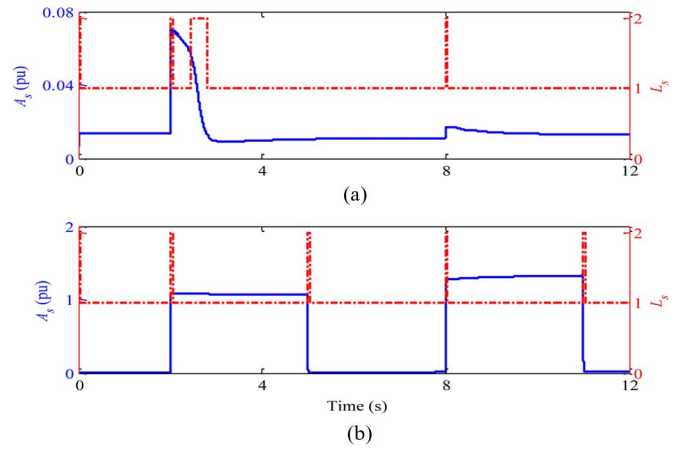


Fig. 10. Responses of estimated amplitudes and algorithms' outputs during: (a) islanding and (b) a three-phase short circuit.

switching of capacitor, and load variations. In Fig. 10(a), an islanding condition is detected subsequent to a transient behavior caused by grid disconnection. The transient behavior is detected locally as well by both DGs ( $L_v^{B,C} = 2$ ) and hence a signal is sent to PCC to check the status of grid. The islanding is detected by PCC within 39.5 ms of occurrence. Also, a transient behavior ( $L_s = L_v^{B,C} = 2$ ) caused by a three-phase short circuit is detected both at PCC and locally by each DG as shown in Fig. 10(b). Since the test region in Fig. 2 is designed to detect fast or switching transient behavior only, the slowly varying grid amplitude afterward is considered as normal operation ( $L_s = 1$ ) as seen in Fig. 10(b). In contrast, a larger period of oscillation is detected locally at both DGs but the PCC-level algorithm declares this case as non-islanding condition. From Fig. 11, a transient behavior is detected locally by both DGs during both on and off switching of induction motor, capacitor, and load. In Fig. 11(a), a sudden drop in voltage is noticed followed by a recovery behavior when the grid reacts by supplying higher current to suppress the voltage drop caused by the startup of induction motor as seen in Fig. 12(a). Both transients caused by induction motor on and off switching are detected locally and similarly the PCC-level algorithm is capable

Fig. 11. Responses of  $\hat{A}_v^{B,C}$  (solid) and  $L_v^{B,C}$  (dash-dotted) during: (a) startup of induction motor and (b) capacitor and load switching.Fig. 12. Responses of  $\hat{A}_s$  (solid) and  $L_s$  (dash-dotted) during: (a) startup of induction motor and (b) capacitor and load switching.

of classifying this case as a non-islanding condition. Similar behavior is noticed for capacitor and load switching. However, a higher  $\hat{A}_s$  value is observed in Fig. 12(b) for both capacitor and load switching. The reason for the high  $\hat{A}_s$  value is that both switching takes place inside the island and hence the grid reacts by absorbing/injecting the power mismatch to support both bus voltages in the island. Therefore, the proposed technique is robust against power system disturbances such as three-phase short circuit, induction motor switching, capacitor switching, and load switching. Compared to the UFP/OFP and UVP/OVP method, the proposed technique relies on instantaneous values and can detect islanding in less than 4 cycles. The proposed technique will require more data to provide fast islanding detection with negligible NDZ.

## IX. CONCLUSION

In this paper, a new IDM is developed, and it involves two dynamic estimators based on the system dynamics during islanding occurrence. The dynamic estimators estimate both amplitudes and phase angles of the current injected by the grid at PCC in addition to the DG's local bus voltage. Analytical and

simulation results show superior performance for the PCC algorithm, especially for high  $Q_f$  values due to the increase in grid current amplitude. In addition, the NDZ of the proposed PCC algorithm is very small and it can be approximated by a single line at 60 Hz for all values of  $Q_f$ . The time required to detect islanding condition is less than four cycles for all the simulated cases. Moreover, a distributed multi-DG algorithm is proposed for generalized multi-DG structure. The distributed algorithm has the ability to detect islanding both locally and at PCC level. In conclusion, the proposed scheme is robust, and the islanding condition can be distinguished from other types of power system disturbances.

## REFERENCES

- [1] *IEEE Recommended Practice for Utility Interface of Photovoltaic (PV) Systems*, IEEE Standard 929-2000, Apr. 2000.
- [2] *Inverters, Converters, and Controllers for Use in Independent Power Systems*, UL Standard 1741, 2002.
- [3] F. De Mango, M. Liserre, and A. D. Aquila, "Overview of anti-islanding algorithms for PV systems Part I: Passive methods," in *Proc. 12th Int. Power Electr. Motion Control Conf.*, Sep. 2006, pp. 1878–1883.
- [4] W. Bower and M. Ropp, "Evaluation of islanding detection methods for photovoltaic utility-interactive power systems," Int. Energy Agency, Rep. IEA-PVPS T5-09:2002, Mar. 2002.
- [5] B. Yu, M. Matsui, and G. Yu, "A review of current anti-islanding methods for photovoltaic power system online, 2010." [Online]. Available: <http://www.sciencedirect.com/science/article/pii/S0038092X10000319>
- [6] F. De Mango, M. Liserre, and A. D. Aquila, "Overview of anti-islanding algorithms for PV systems Part II: Active methods," in *Proc. 12th Int. Power Electr. Motion Control Conf.*, Sep. 2006, pp. 1884–1889.
- [7] H. Karimi, A. Yazdani, and R. Iravani, "Negative sequence current injection for fast islanding detection of a distributed resource unit," *IEEE Trans. Power Electron.*, vol. 23, no. 1, pp. 298–307, Jan. 2008.
- [8] G. Gonzalez and R. Iravani, "Current injection for active islanding detection of electronically-interfaced distributed resources," *IEEE Trans. Power Del.*, vol. 21, no. 3, pp. 1698–1705, Jul. 2006.
- [9] X. Wang and W. Freitas, "Impact of positive-feedback anti-islanding methods on small-signal stability of inverter-based distributed generation," *IEEE Trans. Energy Convers.*, vol. 23, no. 3, pp. 923–931, Sep. 2008.
- [10] V. Menon and M. Nehrir, "A hybrid islanding detection technique using voltage unbalance and frequency set point," *IEEE Trans. Power Syst.*, vol. 22, no. 1, pp. 442–448, Feb. 2007.
- [11] P. Mahat, Z. Chen, and B. Jensen, "A hybrid islanding detection technique using average rate of voltage change and real power shift," *IEEE Trans. Power Del.*, vol. 24, no. 2, pp. 764–771, Apr. 2009.
- [12] Z. Ye, A. Kolwalkar, Y. Zhang, P. Du, and R. Walling, "Evaluation of anti-islanding schemes based on nondetection zone concept," *IEEE Trans. Power Electron.*, vol. 19, no. 5, pp. 1171–1176, Sep. 2004.
- [13] L. Lopes and H. Sun, "Performance assessment of active frequency drifting islanding detection methods," *IEEE Trans. Energy Convers.*, vol. 21, no. 1, pp. 171–180, Mar. 2006.
- [14] M. Ropp, M. Begovic, A. Rohatgi, G. Kern, R. Bonn, and S. Gonzalez, "Determining the relative effectiveness of islanding detection methods using phase criteria and nondetection zones," *IEEE Trans. Energy Convers.*, vol. 15, no. 3, pp. 290–296, Sep. 2000.
- [15] J. Vieira, W. Freitas, W. Xu, and A. Morelato, "An investigation on the nondetection zones of synchronous distributed generation anti-islanding protection," *IEEE Trans. Power Del.*, vol. 23, no. 2, pp. 593–600, Apr. 2008.

- [16] L. Lopes and Y. Zhang, "Islanding detection assessment of multi-inverter systems with active frequency drifting methods," *IEEE Trans. Power Del.*, vol. 23, no. 1, pp. 480–486, Jan. 2008.
- [17] B. Bahrani, H. Karimi, and R. Iravani, "Nondetection zone assessment of an active islanding detection method and its experimental evaluation," *IEEE Trans. Power Del.*, vol. 26, no. 2, pp. 517–525, Apr. 2011.
- [18] M. Al Hosani, Z. Qu, and H. Zeineldin, "Development of current dynamic estimator for islanding detection of inverter based distributed generation," in *Proc. Int. Conf. Power Syst. Technol.*, Oct. 24–28, 2010, pp. 1–8.
- [19] K. M. Vu, *Optimal Discrete Control Theory: The Rational Function Structure Model*. Ottawa, ON, Canada: AuLac Technologies, 2007. [Online]. Available: <http://www.aulactechnologies.com>
- [20] H. Zeineldin and S. Kennedy, "Sandia frequency-shift parameter selection to eliminate nondetection zones," *IEEE Trans. Power Del.*, vol. 24, no. 1, pp. 486–487, Jan. 2009.
- [21] H. Xin, Z. Qu, J. Seuss, and A. Maknouninejad, "A self-organizing strategy for power flow control of photovoltaic generators in a distribution network," *IEEE Trans. Power Syst.*, vol. 26, no. 3, pp. 1462–1473, Aug. 2011.
- [22] W. Kersting, "Radial distribution test feeders," in *Proc. IEEE Power Eng. Soc. Winter Meeting*, 2001, vol. 2, pp. 908–912.



**Mohamed Al Hosani** (S'10–M'13) received the B.Sc. degree in electrical engineering from the American University of Sharjah, United Arab Emirates, in 2008 and the M.Sc. and the Ph.D. degrees in electrical engineering from the University of Central Florida, Orlando, FL, USA, in 2010 and 2013, respectively.

Currently, he is an Assistant Professor with the Masdar Institute, United Arab Emirates. His current interests include the anti-islanding algorithm and microgrid stability analysis.



**Zhihua Qu** (M'90–SM'93–F'09) received the Ph.D. degree in electrical engineering from the Georgia Institute of Technology, Atlanta, GA, USA, in 1990.

Since then, he has been with the University of Central Florida, Orlando, FL, USA. Currently, he is the SAIC Endowed Professor with the College of Engineering and Computer Science, a Professor and the Chair of Electrical and Computer Engineering, and the Director of FEEDER Center (one of DoE-funded national centers on distributed technologies and smart grid). His areas of expertise are nonlinear systems and control, with applications to energy and power systems. In energy systems, his research covers such subjects as low-speed power generation, dynamic stability of distributed power systems, anti-islanding control and protection, distributed generation and load sharing control, distributed VAR compensation, distributed optimization, and cooperative control.



**H. H. Zeineldin** (M'08–SM'13) received the B.Sc. and M.Sc. degrees in electrical engineering from Cairo University, Cairo, Egypt, in 1999 and 2002, respectively, and the Ph.D. degree in electrical and computer engineering from the University of Waterloo, Waterloo, ON, Canada, in 2006.

He is an Associate Professor with the Masdar Institute, United Arab Emirates. He is currently an Editor of the IEEE TRANSACTIONS ON ENERGY CONVERSION and of the IEEE TRANSACTIONS ON SMART GRIDS. His current interests include power system protection, microgrids, and distributed generation.